Comparison of Aerosol Single Scattering Albedos Derived by Diverse Techniques in Two North Atlantic Experiments

P. B. RUSSELL,[a] J. REDEMANN,[b] B. SCHMID,[b] R. W. BERGSTROM,[b] J. M. LIVINGSTON,[c] D. M. MCINTOSH,[d] S. A. RAMIREZ,[d] S. HARTLEY,[e] P. V. HOBBS,[e] P. K. QUINN,[f] C. M. CARRICO,[g,k] M. J. ROOD,[g] E. ÖSTRÖM,[h,l] K. J. NOONE,[h] W. VON HOYNINGEN-HUENE,[i] AND L. REMER[j]

[a]*NASA Ames Research Center, Moffett Field, California*
[b]*Bay Area Environmental Research Institute, San Francisco, California*
[c]*SRI International, Menlo Park, California*
[d]*Symtech Corporation, Moffett Field, California*
[e]*University of Washington, Seattle, Washington*
[f]*NOAA/PMEL, Seattle, Washington*
[g]*University of Illinois at Urbana–Champaign, Urbana, Illinois*
[h]*Stockholm University, Stockholm, Sweden*
[i]*Bremen University, Bremen, Germany*
[j]*NASA Goddard Space Flight Center, Greenbelt, Maryland*

(Manuscript received 9 January 2001, in final form 18 June 2001)

ABSTRACT

Aerosol single scattering albedo ω (the ratio of scattering to extinction) is important in determining aerosol climatic effects, in explaining relationships between calculated and measured radiative fluxes, and in retrieving aerosol optical depths from satellite radiances. Recently, two experiments in the North Atlantic region, the Tropospheric Aerosol Radiative Forcing Observational Experiment (TARFOX) and the Second Aerosol Characterization Experiment (ACE-2), determined aerosol ω by a variety of techniques. The techniques included fitting of calculated to measured radiative fluxes; retrievals of ω from skylight radiances; best fits of complex refractive index to profiles of backscatter, extinction, and size distribution; and in situ measurements of scattering and absorption at the surface and aloft. Both TARFOX and ACE-2 found a fairly wide range of values for ω at midvisible wavelengths (~550 nm), with $0.85 \leq \omega_{\text{midvis}} \leq 0.99$ for the marine aerosol impacted by continental pollution. Frequency distributions of ω could usually be approximated by lognormals in $\omega_{\text{max}} - \omega$, with some occurrence of bimodality, suggesting the influence of different aerosol sources or processing. In both TARFOX and ACE-2, closure tests between measured and calculated radiative fluxes yielded best-fit values of ω_{midvis} of 0.90 ± 0.04 for the polluted boundary layer. Although these results have the virtue of describing the column aerosol unperturbed by sampling, they are subject to questions about representativeness and other uncertainties (e.g., thermal offsets, unknown gas absorption). The other techniques gave larger values for ω_{midvis} for the polluted boundary layer, with a typical result of $\omega_{\text{midvis}} = 0.95 \pm 0.04$. Current uncertainties in ω are large in terms of climate effects. More tests are needed of the consistency among different methods and of humidification effects on ω.

1. Introduction

Aerosol single scattering albedo (SSA) ω (the fraction of intercepted light that is scattered, rather than absorbed) is important in

- determining aerosol climatic effects (e.g., Hansen et al. 1998; Haywood and Shine 1995; Chylek and Wong 1995),
- explaining differences between calculated and measured downwelling radiative fluxes (e.g., Halthore et al. 1998; Kato et al. 1997; Mlawer et al. 2000), and
- determining the relationship between satellite-measured radiance and aerosol optical depth (e.g., Stowe et al. 1997; King et al. 1999; Mishchenko et al. 1999; Durkee et al. 2000).

Because of growing interest in all these topics, two experiments in the North Atlantic region devoted considerable effort to determining aerosol ω. This paper summarizes and compares ω results from these experiments: the 1996 Tropospheric Aerosol Radiative Forcing Observational Experiment [TARFOX (Russell et al.

[k] Current affiliation: Georgia Institute of Technology, Atlanta, Georgia.
[l] Current affiliation: Met Office, Bracknell, Berkshire, United Kingdom.

Corresponding author address: Philip B. Russell, Atmospheric Chemistry and Dynamics Branch, NASA Ames Research Center, MS 245-5, Moffett Field, CA 94035-1000.
E-mail: prussell@mail.arc.nasa.gov

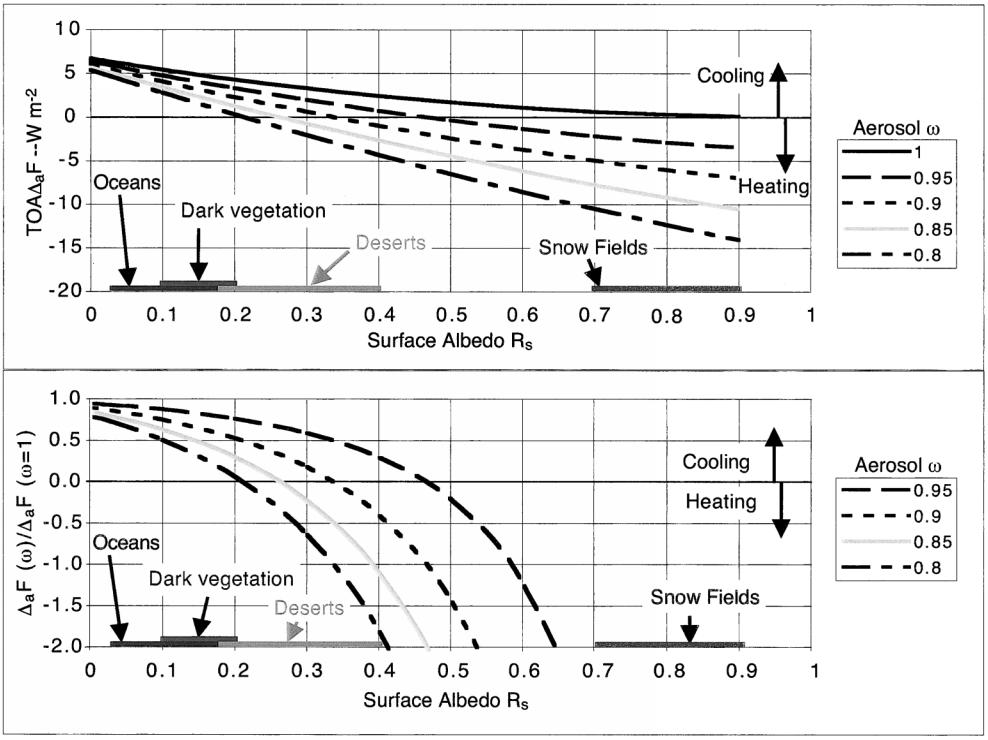

FIG. 1. (a) Aerosol-induced change in top-of-atmosphere upwelling flux $\Delta_a F\uparrow$. Results are from Eq. (1) using AOD = 0.1, aerosol upscatter fraction $\beta_a = 0.17$, no clouds ($A_c = 0$), and atmospheric transmission $T = 0.76$. (b) Ratio of flux change for given aerosol ω to flux change for $\omega = 1$.

1999a)] and the 1997 North Atlantic Aerosol Characterization Experiment [ACE-2 (Raes et al. 2000; Russell and Heintzenberg 2000)]. We focus on results for the atmospheric boundary layer in different situations (e.g., marine versus continental flows, ''clean'' versus polluted conditions). Results in the presence of African dust are not discussed here. We consider the strengths and limitations of the different techniques used, including whether they describe the aerosol in its ambient state or as perturbed by sampling processes; whether they describe the aerosol at the surface, as a function of altitude, or integrated over a column; the ease of acquiring representative datasets; results obtained in tests of consistency with radiative flux changes; and the likelihood of various artifacts and errors.

2. Importance of aerosol single scattering albedo

To illustrate the importance of aerosol ω, we explore briefly the sensitivity of aerosol climate effects and satellite retrievals to assumed values of ω. As an example, Bergstrom and Russell (1999) showed that, over the ocean, for fixed aerosol optical depth (AOD), a change of 0.07 in ω produced a change of 21% in the aerosol-induced radiative flux change at the tropopause. The sensitivity over common land surfaces can be much larger. This is illustrated in Fig. 1, which uses the diurnal average flux-change approximation of Haywood and Shine (1995), Chylek and Wong (1995), and Russell et al. (1997):

$$\Delta_a F\uparrow = \frac{1}{2} F_T T^2 (1 - A_c) \times [\omega\overline{\beta_a}(1 - \overline{R_s})^2 - 2(1 - \omega)\overline{R_s}]\text{AOD}. \quad (1)$$

Here $\Delta_a F\uparrow$ is the aerosol-induced change in upwelling flux at the top of atmosphere, F_T is the solar constant, T is the atmospheric transmission, A_C is the cloud fraction, β_a is the aerosol upscatter fraction, and R_S is the surface albedo. Figure 1 shows that, over dark vegetation, changing ω from 1.0 to 0.9 can reduce $\Delta_a F\uparrow$ by 50% or more. Over deserts and snow fields the same change in ω can reduce $\Delta_a F\uparrow$ by more than 100%, thus changing the sign of the aerosol effect from cooling to heating (see also Sokolik and Toon 1997). Also, flux changes within and below the aerosol layer, which can affect atmospheric stability, heating rates, surface temperatures, and cloud formation and persistence, can be even more sensitive to aerosol ω (e.g., Hansen et al. 1997, 1998; Ackerman et al. 2000; Podgorny et al. 2000). This increased sensitivity can cause the critical single scatter albedo, where cooling shifts to warming, to exceed the values implied by Fig. 1 (which does not consider cloud effects, for example).

The dependence of satellite-retrieved AOD on ω can be illustrated by using the linearized single scattering

approximation (e.g., Stowe et al. 1997; King et al. 1999),

$$\mathrm{AOD}_{\mathrm{SAT}} = 4\mu_0\mu_v \frac{L_a}{\omega P_a(\Psi)}, \quad (2)$$

where L_a is the aerosol contribution to satellite-measured radiance, μ_0 and μ_v are the cosines of the sun and view zenith angles, P_a is the aerosol scattering phase function, and Ψ is the scattering angle. Assessing the full sensitivity of $\mathrm{AOD}_{\mathrm{SAT}}$ to aerosol absorption requires accounting for the fact that ω and P_a are highly correlated, and that changing the aerosol complex refractive index m to change ω can produce even larger changes in $P_a(\Psi)$ at satellite view angles. For example, Stowe et al. (1997) reported that increasing the imaginary part of the aerosol refractive index m_i from 0 to 0.01 in the aerosol model of Ignatov et al. (1995) decreased ω by only 10% but simultaneously decreased $P_a(\Psi)$ by ~30%, thus decreasing their product by ~37% and increasing $\mathrm{AOD}_{\mathrm{SAT}}$ by ~59% [cf. Eq. (2)].

When assessing flux changes by starting with a given satellite radiance L_a, the effect of changing ω (or P_a) on both $\mathrm{AOD}_{\mathrm{SAT}}$ and $\Delta_a F\uparrow$ must be handled in a self-consistent way. This can be illustrated by substituting (2) in (1), yielding

$$\Delta_a F\uparrow = 2F_T T^2(1 - A_c) \times [\omega\overline{\beta_a}(1 - \overline{R_s})^2 - 2(1 - \omega)\overline{R_s}]\mu_0\mu_v \times \frac{L_a}{\omega P_a(\Psi)}. \quad (3)$$

Investigating the sensitivity of (3) to coupled changes in ω and P_a for realistic aerosol models is beyond the scope of this paper. Nevertheless, the above discussion illustrates the importance of the magnitude of aerosol ω in a variety of applications.

3. TARFOX techniques and results

Four techniques were used in TARFOX to determine aerosol ω. One of these techniques derives values for ω as a best-fit parameter when comparing flux changes measured by airborne pyranometer to those computed from aerosol properties (Hignett et al. 1999; Russell et al. 1999b). The computed ω values are wavelength-dependent, deriving from wavelength-dependent complex refractive indices for aqueous sulfate plus a variable imaginary component (see Russell et al. 1999b; Bergstrom and Russell 1999, for details). Calculated flux changes cover the band 300–3000 nm, to match the band of the flux measurements. The best-fit values for ω(550 nm) thus obtained are listed in Table 1a and shown by the data points labeled Ru99, B&R99 in Fig. 2. Some of the strengths of this technique are that it describes the aerosol both in the column (vertically integrated) and in its ambient state, unperturbed by sampling. Also, since the ω values are derived from measured radiative

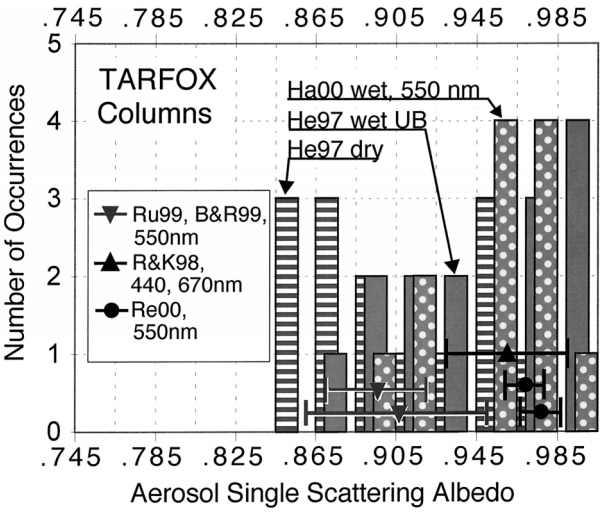

FIG. 2. Column values of aerosol single scattering albedo from TARFOX measurements. Histograms give number of occurrences of aerosol column single scattering albedo values derived from nephelometer and absorption photometer measurements on UW C-131A. He97 = Hegg et al. (1997); Ha00 = Hartley et al. (2000). Data points labeled Ru99 and B&R99 are from best fits to radiative flux measurements (Russell et al. 1999b; Bergstrom and Russell 1999). Data points labeled R&K98 are retrieved from skylight radiance measurements (Remer and Kaufman 1998). Data points labeled Re00 are from best-fit complex refractive indices obtained by Redemann et al. (2000b) by combining vertical profiles of lidar backscatter, sun photometer extinction, and relative particle size distribution. Re00 results, originally given for the 200–700-nm band, were recalculated at 550 nm for this paper.

flux changes, these values should be successful in computing realistic flux changes—as required by climate calculations. However, this also makes the technique dependent on the quality of the flux-change measurements (including such problems as thermal offsets (e.g., Bush et al. 2000; Haeffelin et al. 2001), and on the accuracy of calculations used to separate the effects of aerosols from the effects of any absorbing gases (e.g., water vapor) in the flux-change measurements. Thus, errors in either flux measurements or gas spectroscopy can produce errors in the derived values of aerosol ω. Also, the technique requires special conditions (e.g., little or no clouds) to isolate the aerosol effect. Furthermore, having the pyranometers on an aircraft with other aerosol instruments is desirable to tighten closure (e.g., reduce effects of radiometer offsets by differencing altitudes, provide in situ aerosol chemistry, size, and other properties). The requirement for cloud-free conditions and the desirability of integrated airborne measurements have caused the number of results generated to date to be relatively small. The representativeness of these few results is unknown.

A second technique used in TARFOX retrieved aerosol ω from sun and sky radiance measurements (Remer et al. 1999; Remer and Kaufman 1998), yielding the result labeled R&K98 in Fig. 2 and listed in Table 1a. We obtained the uncertainty of ± 0.03 from Fig. 7c of

Remer and Kaufman (1998), which shows that, at both the 440- and 670-nm wavelengths, $\omega = 0.96$ gives the best fit to measured radiance, but $\omega = 0.93$ and $\omega = 0.99$ are well within the scatter of the data. Like the flux-fitting technique, sun–sky radiance retrievals have the advantage of describing the column aerosol in its unperturbed state. Moreover, sun–sky radiance retrievals are probably less subject to errors caused by inaccurate treatment of absorbing gases. For example, the retrievals use narrowband measurements at 440 and 670 nm—two wavelengths relatively unaffected by gas absorption.

A third technique obtained aerosol ω from best-fit complex refractive indices and aerosol size distributions ($0.1 < D < 47.0$ μm) measured in situ (Redemann et al. 2000b). The refractive indices were first derived as those that best reproduced lidar-derived aerosol backscatter profiles (at wavelength 815 nm) and then compared to sun photometer–derived aerosol optical depths (at 4 wavelengths, 380–1020 nm) in a given layer (Redemann et al. 2000a). In this process, the aerosol size distributions were adjusted iteratively to yield three-way closure between the lidar-derived aerosol backscatter, the sun photometer–derived aerosol optical depth spectra and the same quantities calculated from the adjusted size distributions and refractive indices. To achieve this closure, the adjustment to the aerosol size distributions entailed an iterative increase of the particle sizes in the range of the composite size distributions that used the Forward Scattering Spectrometer Probe–300 particle probe data (i.e., $0.4 < D < 3.2$ μm) by 20% to 68% (independent of size within that range). Redemann et al. (2000a) showed that refractive indices independent of wavelength over the range 380–1020 nm reproduced measured optical depth over that range. These wavelength-independent refractive indices were used to calculate wavelength-dependent values of aerosol ω, which were then averaged over bands of a radiative transfer model. Column-average results for the 200–700-nm band are listed in Table 1a. (This technique also yields vertically resolved ω; see below.) For this paper we have made analogous calculations for the single 550-nm wavelength. These results are also listed in Table 1a and shown by the data points labeled Re00 in Fig. 2. The uncertainties listed and shown are based on a sensitivity analysis that considered the range of real and imaginary refractive indices that produced calculated backscatter and extinction values consistent with measured values and their uncertainties ($\pm 30\%$ for backscatter and extinction), plus a range of size distributions that included both the adjusted and unadjusted ones described above.

The Redemann et al. (2000a,b) technique combines results of in situ size distribution measurements with effects of ambient aerosols on backscatter and extinction measurements. Thus, it is somewhat subject to sampling effects on the in situ size distribution measurements; however, these effects are minimized by using only relative size distributions. Another possible concern is that

TABLE 1a. Aerosol single scattering albedos derived from TARFOX data.

Method	Altitude (km MSL)	Wavelength (nm)	Relative humidity	Number of cases or data points	Aerosol ω		Reference
					Result or mean	Std dev (SD) or uncertainty (U)	
Flux best fit	Layer, 0 to ~3	550	Ambient (~30%–98%)	2	0.895 0.905	0.025 (U) 0.045 (U)	Russell et al. (1999b); Bergstrom and Russell (1999)
Sun–sky radiance retrieval	Column	440, 670	Ambient (~30%–99%)	52[a]	0.96	0.03 (U)	Remer et al. (1999); Remer and Kaufman (1998)
Lidar–sun photometer–size best fit	Layer, 0 to ~3[b]	200–700	Ambient, 63%[c]	2	0.974	0.012 (U)	Redemann et al. (2000b)
		200–700	Ambient, 69%[c]		0.969	0.009 (U)	
		550	Ambient, 63%[c]		0.977	0.010 (U)	
		550	Ambient, 69%[c]		0.969	0.010 (U)	
Nephelometer–absorption photometer	Layer, 0 to ~3[b]	~550	Dry (<30%)	14	0.90	0.04 (SD)	Hegg et al. (1997)
			Wet scat, dry abs[d]	14	0.94	0.04 (SD)	
Nephelometer–absorption photometer	Layer, 0 to ~3[b]	550	Wet scat, est wet abs	12	0.95	0.03 (SD)	Hartley et al. (2000)

[a] 52 cases from TARFOX and the Sulfate, Clouds, and Radiation–Atlantic (SCAR-A) experiment, comparing measured and computed skylight at scattering angles 85°, 120°, and 156°.
[b] Method also yields height-resolved aerosol ω; see references.
[c] Layer average, extinction weighted.
[d] The combination of wet scattering (scat) and dry absorption (abs) gives an upper bound for ambient aerosol ω, for nearly all cases (e.g., Redemann et al. 2001).

TABLE 1b. Aerosol single scattering albedos derived from ACE-2 data.

Method	Altitude (km ASL)	Wavelength (nm)	Relative humidity	Condition	Number of cases or data points	Aerosol ω		Reference
						Result or mean	Std dev (SD) or uncertainty (U)	
Flux best fit	Column	350–3900	Ambient (~25%–85%)	Pollution outbreaks	6	0.90	0.04 (SD)	VHH99
				Clean periods	8	0.98	0.03 (SD)	
Nephelometer–absorption photometer	Layer, 0.03–1	550	<40%	Anthropogenically influenced	4	0.83	0.08 (SD)	Öström and Noone (2000)
			Wet scat, dry abs*	Anthropogenically influenced	4	0.93	+0.03–0.05 (U)	
Nephelometer–absorption photometer	0.01	550	55%	Continental flows (24 days)	677	0.95	0.04 (SD)	Quinn et al. (2000)
				Marine flows (7 days)	242	0.98	0.02 (SD)	
Nephelometer–aethalometer	0.05	550	27%	Pollution outbreaks (~23 days)	1505	0.94	0.03 (SD)	Carrico et al. (2000)
			27%	Clean periods (~15 days)	966	0.93	0.05 (SD)	
			82%	Pollution outbreaks (~23 days)	1505	0.95	0.02 (SD)	
			82%	Clean periods (~15 days)	966	0.95	0.03 (SD)	

* The combination of wet scattering and dry absorption gives an upper bound for ambient ω, for nearly all cases (e.g., Redemann et al. 2001).

the analyses assume spherical aerosols. Because aerosol asphericity generally reduces backscatter, as does aerosol absorption, occurrence of aspherical aerosols could lead to overestimates of absorption (underestimates of ω). However, during TARFOX, the aerosol layers that contributed most to column backscatter or extinction had high relative humidity (typical values 60%–99%) and large liquid water content. [For example, liquid water was the single largest contributor to aerosol extinction, contributing, on average, 35% of aerosol extinction (Hegg et al. 1997), more than either organics or sulfates.] Hence asphericity is expected to have little effect on aerosol ω derived by this technique in TARFOX. This is borne out by the results obtained for ω, which have relatively large values (Fig. 2 and Table 1a).

A fourth technique used in TARFOX was to combine airborne measurements of aerosol scattering and absorption by nephelometer and absorption photometer (Hegg et al. 1997). This technique yields aerosol ω at flight sampling altitudes, which can be averaged over layers. Layer-averaged results for dry (RH $\leqslant$ 30%) aerosols are shown by the histogram in Fig. 2 labeled ''He97 dry.'' The histogram labeled ''He97 wet UB'' gives analogous results obtained by combining absorption measurements for dry aerosols with scattering coefficients adjusted to the ambient humidity. Upper bound (UB) is included in the label, since, as shown by Redemann et al. (2001) combining dry absorption with wet scattering gives an upper bound for ambient ω in nearly all cases. As described in more detail by Hegg et al. (1997), the scattering humidification factors were measured by varying the humidity of aerosol collected by a bag sampler aboard the aircraft; scattering was measured by an ME Electron nephelometer, and absorption by a Radiance Research aerosol absorption photometer.

A reanalysis by Hartley et al. (2000) of a subset of the Hegg et al. (1997) airborne nephelometer and absorption photometer measurements yielded the histograms labeled ''Ha00'' in Fig. 2. This reanalysis estimated absorption humidification factors as the average of unity and the corresponding scattering humidification factor, with an uncertainty spanning these two limits. It also excluded two of the 14 profiles used by Hegg et al. (1997) and reprocessed the dry absorption values (see Hartley et al. 2000, for details). Means and standard deviations of the Hegg et al. (1997) and Hartley et al. (2000) layer-averaged results are listed in Table 1a. Hartley et al. (2000) also derived vertical profiles of ω. Figures 2 and 6 of Redemann et al. (2000b) compare example vertically resolved results from Hartley et al. with corresponding results from the Redemann et al. (2000b) technique. Agreement is shown to be within the uncertainties of the techniques (typically ± 0.02 to ± 0.04).

Strengths of the airborne nephelometer–absorption photometer technique include its ability to produce frequent measurements of aerosol scattering and absorption

at flight altitudes, which can yield vertical profiles or layer-averaged values for aerosol ω. Also, the resulting measurements of light scattering and absorption (the two components used to calculate SSA) provide a more direct measurement of SSA than the preceding techniques. Limitations result from the fact that aerosols are sampled through an inlet at aircraft speeds, generally resulting in some aerosol loss. The most common losses are 1) aerodynamic separation of large particles from the sampling stream and 2) possible evaporation of volatile components, such as water, organics, and nitrates. Aerodynamic separation can be minimized by designing the inlet to have negligible losses for the particle sizes that dominate extinction. Effects of water loss on the nephelometer scattering measurements can be compensated by measuring RH in the scattering chamber and using measured scattering humidification factors to adjust results to ambient RH (e.g., Hegg et al. 1997; Hartley et al. 2000). More difficult to quantify and allow for are the effects of organic and nitrate loss on scattering; and the effect of water, organic, and nitrate loss on absorption. As a consequence these effects are usually not taken into account; however, Bergin et al. (1997) have described ammonium nitrate aerosol evaporation in a heated nephelometer. A disadvantage of the measurement of light absorption by the absorption photometers used in TARFOX and ACE-2 is that they measure attenuation of a filter-deposited sample rather than the aerosol in its freely suspended state (e.g., Bond et al. 1999).

4. ACE-2 techniques and results

In ACE-2 aerosol ω was determined both as a best-fit parameter when comparing measured and calculated flux changes at the surface (von Hoyningen-Huene, 1999, personal communication; hereafter VHH99) and by combining nephelometer and absorption photometer measurements. The nephelometer–absorption photometer results were obtained on the ACE-2 ship (10 m ASL), at the Sagres, Portugal site (50 m MSL), and on the Pelican aircraft (~30–3900 m MSL).

The nephelometer–absorption photometer results from the ACE-2 ship (Quinn et al. 2000) are shown by the histograms in Fig. 3 and are listed in Table 1b. Results are given for the measurement RH, 55%. Performance characteristics of the Thermo Systems, Inc. (TSI) nephelometer used by Quinn et al. (and also by Carrico et al. 2000, see below) are described by Anderson et al. (1996). Absorption coefficients, determined with a particle soot absorption photometer (PSAP, Radiance Research) were corrected by Quinn et al. for a small (1%–1.5%) positive artifact caused by instrumental interpretation of scattering as absorption using the method of Bond et al. (1999). Measurements were made on particles with aerodynamic diameters less than 10 μm.

Analogous results from the Sagres, Portugal, site

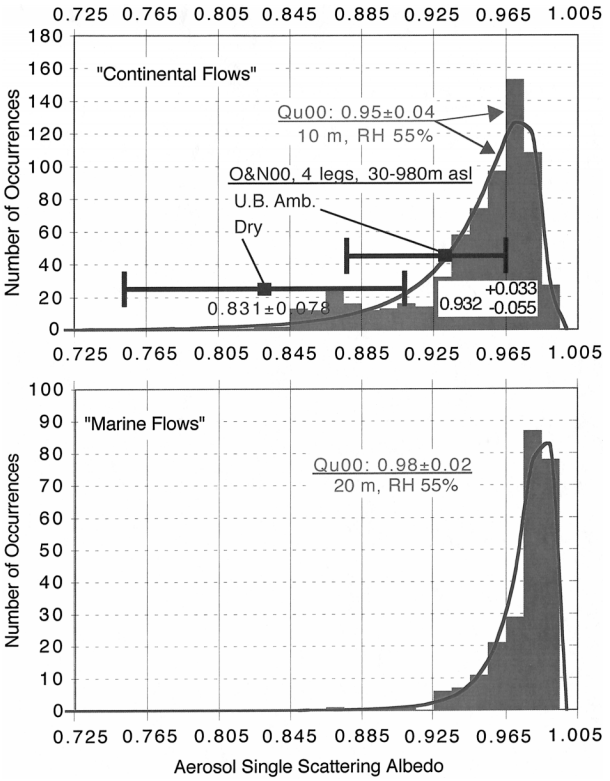

FIG. 3. Histograms and fitted curves give frequency of occurrence of aerosol single scattering albedo values derived from nephelometer and absorption photometer measurements on R/V *Vodyanitsky* in ACE-2 (Jun–Jul 1997, z = 10 m MSL, RH = 55%, $D_{50,\text{aero}}$ = 10 μm, λ = 550 nm) by Quinn et al. (2000). Data points labeled O&N00 are from nephelometer and absorption photometer measurements on Pelican A/C by Öström and Noone (2000).

(Carrico et al. 2000) are shown in Fig. 4 and listed in Table 1b. In this case the measurement RH for scattering coefficients σ_{sp} was varied from 27% to 82%. Absorption coefficients σ_{ap} were measured with an aethalometer assuming a black carbon specific absorption of 10 $m^2\ g^{-1}$ at 550 nm. Because scattering effects in the aethalometer have not been characterized (like the Bond et al. 1999 study for the PSAP), Carrico et al. did not apply a scattering correction to absorption. However, they included this effect in their uncertainty analyses. The aethalometer sampled particles with aerodynamic diameters less than 10 μm at RH $\leq$ 40%.

Results from airborne nephelometer–absorption photometer measurements (Öström and Noone 2000) on four Pelican flight legs within the anthropogenically influenced boundary layer are shown by the data points labeled ''O&N00'' in Fig. 3 and are listed in Table 1b. Öström and Noone determined absorption coefficients with a PSAP and corrected for the scattering artifact using the factors determined by Bond et al. (1999). Air was sampled through an isokinetic inlet and cyclonic impactors that rejected larger particles, with a nominal 50% cutoff at aerodynamic diameter D_a = 2.5 μm. After sampling, air was heated to maintain RH below 40%

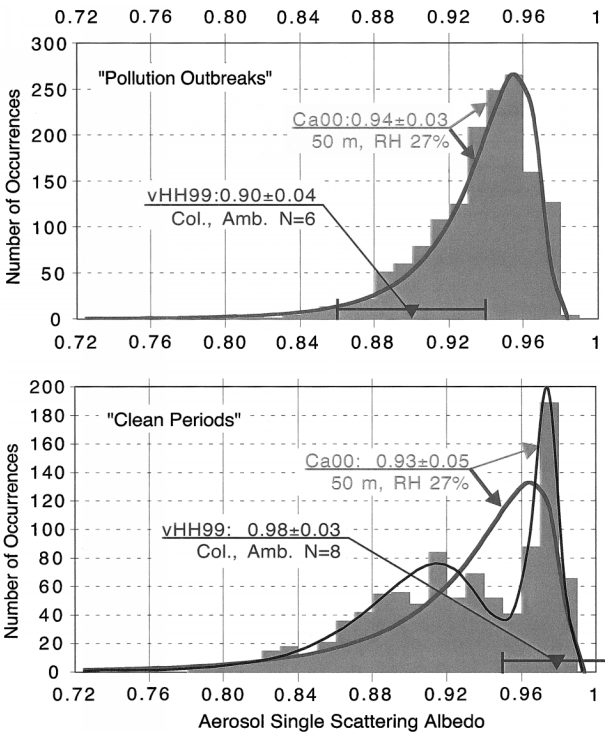

FIG. 4. Histograms and fitted curves give frequency of occurrence of aerosol single scattering albedo values derived from nephelometer and aethalometer measurements at Sagres, Portugal, in ACE-2 (Jun–Jul 1997, z = 50 m MSL, RH = 27%, λ = 550 nm) by Carrico et al. (2000). Data points labeled vHH99 are best fits from flux-change analyses by von Hoyningen-Huene et al. (VHH99).

(below 30% for most measurements). The data point labeled ''U.B. Amb.'' in Fig. 3 combines ''dry'' absorption coefficients (i.e., at measurement RH) with measured scattering coefficients multiplied by a scattering humidification factor, $\sigma_{sp}(80\%)/\sigma_{sp}(30\%)$. As noted above, Redemann et al. (2001) show that this technique gives an upper bound for ambient aerosol ω in nearly all cases. Öström and Noone (2000) used the approximation $\sigma_{sp}(80\%)/\sigma_{sp}(30\%) = [D(80\%)/D(30\%)]^2 = \mathrm{GF}^2$, where GF is the diameter growth factor. The data point and upper uncertainty bar in Fig. 3 use GF = 1.7 (i.e., $\sigma_{sp}(80\%)/\sigma_{sp}(30\%) = 2.9$), one of the largest values reported for the anthropogenically influenced marine boundary layer in several studies (e.g., Kotchenruther et al. 1999; Swietlicki et al. 2000). The lower uncertainty bar uses GF = 1.43, the value obtained from the mean $\sigma_{sp}(80\%)/\sigma_{sp}(30\%) = 2.04$ found by Gassó et al. (2000) on Pelican flight legs within the polluted marine boundary layer in ACE-2. Note that Carrico et al. (2000) found even smaller values during both polluted and clean periods at the Sagres site. Specifically, they found $\sigma_{sp}(82\%)/\sigma_{sp}(27\%) = 1.46 \pm 0.10$ (corresponding to GF(82%, 27%) = 1.21 ± 0.04) during polluted periods and $\sigma_{sp}(82\%)/\sigma_{sp}(27\%) = 1.69 \pm 0.16$ (corresponding to GF(82%, 27%) = 1.30 ± 0.06) during clean periods.

The flux best-fit results of VHH99 for the six polluted and eight clean cases are shown by the data points labeled ''vHH99'' in Fig. 4. Means and standard deviations for all are listed in Table 1b. The effective wavelength of the von Hoyningen-Huene results bears discussion, because these results are from broadband pyranometers (covering 350–3900 nm; cf. Table 1b), and, unlike the TARFOX flux-fitting results (Hignett et al. 1999; Russell et al. 1999b), von Hoyningen-Huene did not derive spectrally resolved best-fit ω using an aerosol model. Nevertheless, we argue that the effective wavelength of the von Hoyningen-Huene flux-fit result is close to 550 nm. The solar energy spectrum peaks at 550 nm. It does have a long infrared tail, which puts half of solar energy longward of ~700 nm, both at the surface and above the atmosphere (Blanchet 1982; Kiehl and Briegleb 1993; Russell et al. 1997). However, this longer-wavelength solar energy is scattered and absorbed by aerosols less than solar energy shortward of 700 nm, because aerosol scattering and absorption decrease with wavelength in this region. To quantify this effect, we have run simulations taking into account the shape of the solar energy spectrum and a realistic range of wavelength dependences for aerosol scattering and absorption. Results of these simulations show that, for a broadband pyranometer covering 350–3900 nm, the effective wavelength for extinction rarely differs from 550 nm by more than 100 nm. In turn, the single scattering albedo at this effective wavelength rarely differs from that at 550 nm by more than 0.01. For example, the seven models of absorbing sulfate aerosols used by Russell et al. (1999b) had $\omega(550\text{ nm}) - \omega(650\text{ nm}) = 0.004 \pm 0.003$. The weak wavelength dependence of ω for polluted boundary layer aerosols in this spectral region is also borne out by the Remer measurements at 440 and 670 nm (Table 1a) and by the small difference between the Redemann results at 550 nm and averaged over the 200–700-nm band (Table 1a). Thus we argue that the effective wavelength for all ω reported in this paper is in the midvisible (~550 nm) and we adopt the symbol ω_{midvis} to describe them.

Curves drawn over the histograms in Figs. 3 and 4 are lognormals in $\omega_{\max} - \omega$; that is,

$$n(a) = \frac{N}{a\sigma_g\sqrt{2\pi}} \exp\left[-\frac{1}{2}\left(\frac{\ln a - \ln a_g}{\sigma_g}\right)^2\right], \quad (4)$$

where

$$a \equiv \omega_{\max} - \omega, \quad (5)$$

N is the number of observations, a_g and σ_g are the geometric mean and standard deviation defined by

$$\ln a_g \equiv \frac{1}{N}\sum_{i=1}^{N} \ln a_i, \quad \text{and} \quad (6a)$$

$$\sigma_g \equiv \sqrt{2[\ln \overline{a} - \ln a_g]}, \quad (6b)$$

and $\overline{a}$ is the arithmetic mean of a. The parameters of the distributions are given in Table 2.

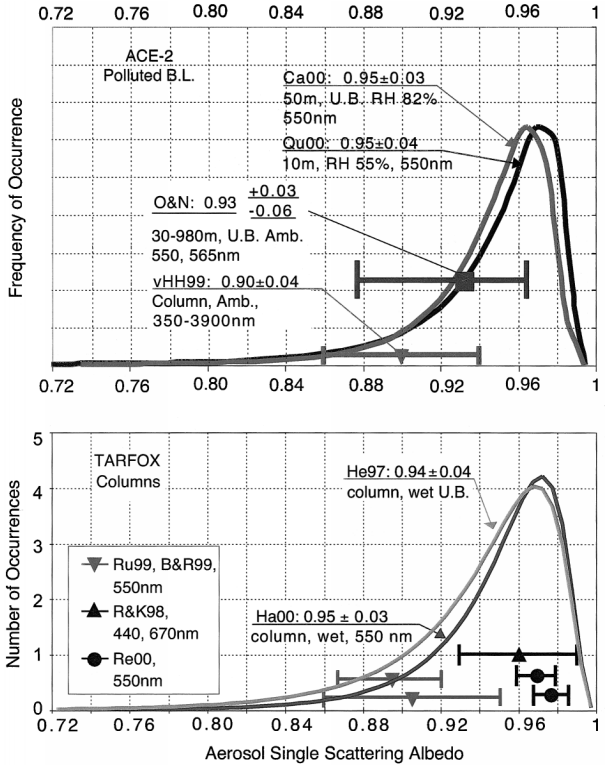

FIG. 5. Comparison of aerosol single scattering albedo distributions and data points for ACE-2 anthropogenically influenced boundary layer cases and for TARFOX columns.

Because the histogram for ''clean periods'' in Fig. 4 appears bimodal, we have also derived lognormal parameters for each mode. These parameters are also given in Table 2, and the bimodal curve is shown in Fig. 4. It captures the bimodal shape of the clean periods histogram fairly well. The TARFOX histograms in Fig. 2 also suggest bimodality. For completeness we show the corresponding bimodal lognormal parameters in Table 2. However, because the numbers of cases are small for these TARFOX column results (14 for Hegg et al. 1997; 12 for Hartley et al. 2000), the apparent bimodality is likely to be a statistical artifact. Therefore, we use only the unimodal parameters for these TARFOX cases.

For the ACE-2 anthropogenically influenced boundary layer cases, lognormal distribution curves are shown in the upper frame of Fig. 5 to facilitate comparison to the TARFOX results, which are shown in the bottom frame. The curve labeled ''Qu00'' is the same as that shown in Fig. 3. The curve labeled ''Ca00'' in Fig. 5 has the same width σ_g as that in Fig. 4, but its geometric mean a_g has been decreased [i.e., peak ω increased; cf. Eq. (5)] by 0.01 to reflect the 0.01 difference between the Carrico et al. (2000) results for polluted conditions at RH of 27% and 82%, respectively (see Table 1b).

5. Discussion and conclusions

Perhaps the most fundamental result of the above comparisons is that both TARFOX and ACE-2 found

TABLE 2a. Parameters of lognormals used to approximate histograms for TARFOX data.

Histogram		N	ω_{max}	a_g	σ_g
He97 wet UB	Unimodal	14	1	0.052	0.662
	Bimodal, small ω	7	1	0.099	0.203
	Bimodal, large ω	7	1	0.027	0.268
Ha00 wet	Unimodal	12	1	0.044	0.617
	Bimodal, small ω	3	1	0.101	0.046
	Bimodal, large ω	9	1	0.034	0.482

the range of aerosol single scattering albedo to be broad. For the ambient, anthropogenically influenced aerosol, both experiments found aerosol single scattering albedos at midvisible wavelengths (~550 nm) distributed throughout the range $0.85 \leq \omega_{midvis} \leq 0.99$ (cf. Fig. 5). When measurements were made in sufficient numbers, distributions could usually be well approximated by lognormals in $\omega_{max} - \omega$, with some occurrence of bimodality, suggesting the influence of different sources and/or processes.

A striking result is the tendency of both the TARFOX and ACE-2 results for the polluted boundary layer to cluster into two groups depending on the technique used to derive aerosol ω. Specifically, in both experiments, closure tests between measured and calculated broadband radiative fluxes yielded best-fit values of ω_{midvis} of 0.90 ± 0.04 for the polluted boundary layer. All the other techniques (skylight retrieval, refractive index fitting to lidar–sun photometer–size profiles, nephelometer–absorption photometer measurements) gave larger ω_{midvis} for the polluted boundary layer. For example, in TARFOX, the column- or layer-averaged results were 0.96 ± 0.03 for skylight retrievals (Remer et al. 1999; Remer and Kaufman 1998), 0.97 ± 0.01 for lidar–sun photometer–size fitting (Redemann et al. 2000a,b), 0.94 ± 0.04 for humidified nephelometer–absorption photometer measurements (Hegg et al. 1997), and 0.95 ± 0.03 for a reanalysis (Hartley et al. 2000) of 12 of the 14 profiles analyzed by Hegg et al. (1997). In ACE-2, the anthropogenically influenced boundary layer results from airborne nephelometer and absorption photometer yielded 0.93 ± 0.05 (or +0.03, −0.06) (Öström and Noone 2000). Measurements by ship- and ground-based nephelometer and absorption photometer yielded 0.95 ± 0.04 at RH 55% (Quinn et al. 2000) and 0.95 ± 0.03 at RH 82% (Carrico et al. 2000).

In assessing the significance of this difference (0.90 ± 0.04 for the flux-based results, ~0.95 ± 0.04 for the others) it is instructive to consider both the range or uncertainty within each group and the strengths and limitations of each technique. First note that, since the values to the right of the ± sign are either 1 standard deviation or 1σ uncertainties, there is a significant overlap and hence a significant chance that the two groups of results could have been drawn from the same population. In other words, the difference between the two groups may not be significant at all. In part this reflects

TABLE 2b. Parameters of lognormals used to approximate histograms for ACE-2 data.

Histogram		N	ω_{max}	a_g	σ_g
Qu00, continental flows		677	0.996	0.037	0.728
Qu00, marine flows		242	1	0.020	0.623
Ca00, pollution outbreaks		1506	0.985	0.041	0.603
Ca00, clean periods	Unimodal	966	0.995	0.051	0.748
	Bimodal, small ω	586	0.995	0.091	0.366
	Bimodal, large ω	380	0.995	0.021	0.376

the small number of results from the flux-fitting technique (two for the polluted boundary layer in TARFOX; six for the polluted column in ACE-2) and the considerable range of results from the other techniques. (In fact, the frequent skewness of the ω histograms means that the std dev by itself can give a mistaken impression of the extent of the small-ω tail of the distribution; cf. Figs. 3 and 4.)

Nevertheless, it is instructive to consider possible reasons for the difference among techniques, assuming that it is significant. One possible reason, mentioned in section 3, is the influence of assumed gaseous absorption on best-fit ω. If gas absorption is underestimated when calculating flux changes, aerosol absorption will be overestimated when calculated fluxes are adjusted to match measured fluxes. In fact, the subject of gas absorption spectroscopy and its role in comparing calculated to measured fluxes is the focus of very active research now, with a wide range of results reported (e.g., Halthore et al. 1998; Giver et al. 2000; Pilewskie et al. 2000; Belmiloud et al. 2000; Mlawer et al. 2000). The accuracy of radiative flux measurements, including corrections for thermal offsets (e.g., Bush et al. 2000; Haeffelin et al. 2001) is also the focus of active research. The magnitude of such corrections ($\sim$5 to $\sim$20 W m^{-2}) is large enough that they might influence aerosol ω values derived by the flux-fitting technique. However, since fluxes input to this technique are differences between fluxes with and without aerosols (either measured or modeled—e.g., Hignett et al. 1999; VHH99), careful consideration of the difference in thermal offsets is needed for specific experimental conditions and procedures (e.g., comparing fluxes measured at different altitudes, comparing fluxes measured on different days, or comparing measured fluxes to model calculations). For example, the fact that VHH99 found $\omega = 0.98 \pm 0.03$ for clean periods (Table 1b, Fig. 3) suggests that thermal offsets have been accounted for appropriately, since thermal offsets significantly larger than they used would yield $\omega > 1$ (negative aerosol absorption).

There are also reasons for potential biases in the other techniques. For example, as mentioned above, absorption is often assumed independent of humidity when ambient aerosol ω is estimated from nephelometer and absorption photometer measurements made at reduced humidity. In fact, as recently emphasized by Redemann et al. (2001), when aerosol black carbon occurs as an inclusion in a sulfate shell, humidity increases can increase absorption. This occurs because the shell focuses the electromagnetic field on the carbon, and shell growth in rising humidity increases the focused field strength. Calculations of this effect for realistic size distributions, humidities, and carbon–sulfate ratios show that, for the range of ω found in TARFOX and ACE-2 (i.e., $0.85 \leq \omega_{midvis} \leq 0.99$), the assumption that absorption is humidity-independent may overestimate ω by $\sim$0.02 (more for smaller dry particles in narrow size distributions, less for larger particles in broad distributions). Fuller et al. (1999) pointed out that shell–core particle morphology as assumed by Redemann et al. (2001) can lead to an overestimate of aerosol light absorption by up to 15% in comparison to calculations assuming random placement of soot agglomerates within the host particles. However, since Redemann et al. (2001) quantified relative statements such as the increase in absorption of a humidified particle relative to its dry state and since the potential overestimate in particle absorption applies to both the dry and the wet particles, the error in single scattering albedo estimates induced by assuming the shell–core particle morphology is probably negligible. As noted in Tables 1a and 1b, this assumption was used in nephelometer–absorption photometer results reported by Hegg et al. (1997), Öström and Noone (2000), and Carrico et al (2000). Reducing those results by $\sim$0.02 does indeed move them significantly toward the flux-fit results of 0.90 ± 0.04 for the polluted boundary layer.

Sampling-inlet effects should also be considered. For example, the inlet on the ACE-2 Pelican aircraft, used by Öström and Noone (2000), rejected larger particles, with a nominal 50% cutoff at aerodynamic diameter $D_a = 2.5$ μm. For typical boundary layer aerosol densities of 1.3 g cm^{-3} (at RH $\sim$80%), this aerodynamic diameter corresponds to a geometric diameter of 2.2 μm. In contrast, the inlet on the ship that produced the Quinn et al. (2000) results in Fig. 3 had an aerodynamic cutoff of 10 μm. Thus, it is highly likely that the aerosol sampled by Öström and Noone had a smaller salt fraction than that sampled by Quinn et al. On the other hand, the salt fraction at the 10-m altitude sampled by Quinn et al. is likely to exceed that averaged over the boundary layer, because of gravitational sedimentation of the largest particles.

6. Implications for future studies

It is worth emphasizing that the difference between the two clusters of results (flux-based and all others) is

large in terms of climate effects. As shown by Fig. 1, changing the value of aerosol ω from 0.95 to 0.90 can reduce tropospheric cooling by ~40% over dark vegetation, and can change the sign of the aerosol effect from cooling to heating over some desert surfaces and over snow fields. Effects on radiant fluxes at the surface and within the boundary layer—which influence convection, cloud formation and persistence, and other processes—can be even larger. Thus further research is warranted to determine whether the difference (between 0.90 ± 0.04 and 0.95 ± 0.04) is indeed significant and, if so, the reasons for it.

One promising avenue is to conduct comparisons between the different techniques that are both more numerous (to cover a representative range of atmospheric conditions and achieve statistical significance) and more carefully controlled. An important criterion is that the aerosols sampled, probed, or described by the different techniques be 1) the same and 2) as close as possible to their ambient state (unperturbed by sampling processes). Thus, in situ results that are compared to flux-change results must describe the aerosol 1) throughout the same layer or column that determines the flux change, and 2) in its ambient state (using accurate correction procedures as necessary). The first requirement points to a need for airborne in situ sampling. In turn, the increased importance of inlet effects (including aerodynamic size separation and evaporation) at aircraft speeds calls for increased effort to understand and minimize these effects, as well as to quantify correction factors. Conversely, care must be taken that the flux-change and optical-depth measurements span the same layer or column as is sampled in situ. This can be achieved by flying a vertical profile using a single airborne platform for in situ sampling, flux radiometry, and solar beam transmissometry; or by careful coordination among two or more airborne platforms. Necessary quality control of the airborne flux radiometer measurements includes careful calibration as well as minimization and measurement of radiometer tilt and temperature effects. Control of radiometer tilt has definite implications for the type of vertical profiles flown (e.g., horizontal legs and ramps versus spirals). Related considerations apply to the airborne solar beam transmission measurements, depending on technique (e.g., tracking sun photometer versus shadowband radiometer). As mentioned in sections 3 and 5, there is also a need for renewed attention to the gas spectroscopy that is used to separate aerosol and gas effects on measured fluxes. Spectrally resolved flux closure tests could provide multiple benefits, including reducing dependence on gas spectroscopy, testing for and isolating other perturbing factors (e.g., clouds, surface albedo), and producing wavelength-dependent values of ω.

Another area worthy of increased attention is quantifying the effects of humidity changes on aerosol absorption. Measuring these effects is difficult, if not impossible, with many current instruments. However, photoacoustic measurements (e.g., Bruce 1991; Moosmuller et al. 1998) may offer promise here. Although vibration sensitivity may preclude airborne photoacoustic measurements, surface measurements may be useful to reveal the important effects and provide data for comparison with, for example, shell-and-core calculations (e.g., Redemann et al. 2001).

Acknowledgments. This research was conducted as part of the Global Aerosol Climatology Program (GACP), the Tropospheric Aerosol Radiative Forcing Observational Experiment (TARFOX), and the second Aerosol Characterization Experiment (ACE-2). TARFOX and ACE-2 are contributions to the International Global Atmospheric Chemistry (IGAC) core project of the International Geosphere-Biosphere Programme (IGBP), and are parts of the IGAC Focus on Atmospheric Aerosols (FAA). GACP is supported by the Radiation Science Program Office of the U.S. National Aeronautics and Space Administration. Other support was provided by the U.S. National Oceanographic and Atmospheric Administration Office of Global Programs, and the U.S. National Science Foundation.

REFERENCES

Ackerman, A. S., O. B. Toon, D. E. Stevens, A. J. Heymsfield, V. Ramanathan, and E. J. Welton, 2000: Reduction of tropical cloudiness by soot. *Science,* **288,** 1042–1047.

Anderson, T. L., and Coauthors, 1996: Performance characteristics of a high sensitivity, three wavelength, total scatter/backscatter nephelometer. *J. Atmos. Oceanic Technol.,* **13,** 967–986.

Belmiloud, D., R. Schermaul, K. Smith, N. Zobov, J. W. Brault, R. C. M. Learner, D. A. Newnham, and J. Tennyson, 2000: New studies of the visible and near-infrared absorption by water vapor and some problems with the HITRAN database. *Geophys. Res. Lett.,* **27,** 3703–3706.

Bergin, M. H., J. A. Ogren, S. E. Schwartz, and L. M. McInnes, 1997: Evaporation of ammonium nitrate aerosol in a heated nephelometer: Implications for field measurements. *Environ. Sci. Technol.,* **31,** 2878–2883.

Bergstrom, R. W., and P. B. Russell, 1999: Estimation of aerosol radiative effects over the mid-latitude North Atlantic region from satellite and in situ measurements. *Geophys. Res. Lett.,* **26,** 1731–1734.

Blanchet, J. P., 1982: Application of Chandrasekhar mean to aerosol optical properties. *Atmos.–Ocean,* **20,** 189–206.

Bond, T. C., T. L. Anderson, and D. Campbell, 1999: Calibration and intercomparison of filter-based measurements of visible light absorption by aerosols. *Aerosol Sci. Technol.,* **30,** 582–600.

Bruce, C. W., T. F. Stromberg, K. P. Gurton, and J. B. Mozer, 1991: Trans-spectral absorption and scattering of electromagnetic radiation by diesel soot. *Appl. Opt.,* **30,** 1537–1546.

Bush, B. C., F. P. J. Valero, A. S. Simpson, and L. Bignone, 2000: Characterization of thermal effects in pyranometers: A data correction algorithm for improved measurement of surface insolation. *J. Atmos. Oceanic Technol.,* **17,** 165–175.

Carrico, C. M., M. J. Rood, J. A. Ogren, C. Neusüß, A. Wiedensohler, and J. Heintzenberg, 2000: Aerosol light scattering properties measured at Sagres, Portugal, during ACE-2. *Tellus,* **52B,** 694–715.

Chylek, P., and J. Wong, 1995: Effect of absorbing aerosols on global radiation budget. *Geophys. Res. Lett.,* **22,** 929–931.

Durkee, P. A., and Coauthors, 2000: Regional aerosol properties from

satellite observation: ACE-1, TARFOX and ACE-2 results. *Tellus,* **52B,** 484–497.

Fuller, K. A., W. C. Malm, and S. M. Kreidenweis, 1999: Effects of mixing on extinction by carbonaceous particles. *J. Geophys. Res.,* **104,** 15 941–15 954.

Gassó, S., and Coauthors, 2000: Influence of humidity on the aerosol scattering coefficient and its effect on the upwelling radiance during ACE-2. *Tellus,* **52B,** 546–567.

Giver, L. P., C. Chackerian Jr., and P. Varanasi, 2000: Visible and near-infrared H_2 ^{16}O line intensity corrections for HITRAN-96. *J. Quant. Spectrosc. Radiat. Transfer,* **66,** 101–105.

Haeffelin, M., S. Kato, A. M. Smith, C. K. Rutledge, T. P. Charlock, and J. R. Mahan, 2001: Determination of the thermal offset of the Eppley precision spectral pyranometer. *Appl. Opt.,* **40,** 472–484.

Halthore, R. N., S. Nemesure, S. E. Schwartz, D. G. Imre, A. Berk, E. G. Dutton, and M. H. Bergin, 1998: Models overestimate diffuse clear-sky surface irradiance: A case for excess atmospheric absorption. *Geophys. Res. Lett.,* **25,** 3591–3594.

Hansen, J., M. Sato, and R. Ruedy, 1997: Radiative forcing and climate response. *J. Geophys. Res.,* **102,** 6831–6864.

——, ——, A. Lacis, R. Ruedy, I. Tegen, and E. Matthews, 1998: Climate forcings in the industrial era. *Proc. Natl. Acad. Sci. USA,* **95,** 12 753–12 758.

Hartley, W. S., P. V. Hobbs, J. L. Ross, P. B. Russell, and J. M. Livingston, 2000: Properties of aerosols aloft relevant to direct radiative forcing off the mid-Atlantic coast of the United States. *J. Geophys. Res.,* **105,** 9859–9885.

Haywood, J. M., and K. P. Shine, 1995: The effect of anthropogenic sulfate and soot aerosol on the clear sky planetary radiation budget. *Geophys. Res. Lett.,* **22,** 603–606.

Hegg, D. A., J. Livingston, P. V. Hobbs, T. Novakov, and P. Russell, 1997: Chemical apportionment of aerosol column optical depth off the mid-Atlantic coast of the United States. *J. Geophys. Res.,* **102,** 25 293–25 303.

Hignett, P., J. P. Taylor, P. N. Francis, and M. D. Glew, 1999: Comparison of observed and modelled direct aerosol forcing during TARFOX. *J. Geophys. Res.,* **104,** 2279–2288.

Ignatov, A., L. Stowe, S. Sakherin, and G. Korotaev, 1995: Validation of the NOAA/NESDIS satellite aerosol product over the North Atlantic in 1989. *J. Geophys. Res.,* **100,** 5123–5132.

Kato, S., T. P. Ackerman, E. E. Clothiaux, J. H. Mather, G. G. Mace, M. L. Wesely, F. Murcray, and J. Michalsky, 1997: Uncertainties in modeled and measured clear-sky surface shortwave irradiances. *J. Geophys. Res.,* **102,** 25 881–25 898.

Kiehl, J. T., and B. P. Briegleb, 1993: The relative roles of sulfate aerosols and greenhouse gases in climate forcing. *Science,* **260,** 311–314.

King, M. D., Y. J. Kaufman, D. Tanré, and T. Nakajima, 1999: Remote sensing of tropospheric aerosols from space: Past, present, and future. *Bull. Amer. Meteor. Soc.,* **80,** 2229–2259.

Kotchenruther, R. A., P. V. Hobbs, and D. A. Hegg, 1999: Humidification factors for atmospheric aerosol off the mid-Atlantic coast of United States. *J. Geophys. Res.,* **104,** 2239–2251.

Mishchenko, M. I., I. G. Geogdzhayev, B. Cairns, W. B. Rossow, and A. A. Lacis, 1999: Aerosol retrievals over the ocean using channel 1 and 2 AVHRR data: A sensitivity analysis and preliminary results. *Appl. Opt.,* **38,** 7325–7341.

Mlawer, E. J., P. D. Brown, S. A. Clough, L. C. Harrison, J. J. Michalsky, P. W. Kiedron, and T. Shippert, 2000: Comparison of spectral direct and diffuse solar irradiance measurements and calculations for cloud-free conditions. *Geophys. Res. Lett.,* **27,** 2653–2656.

Moosmuller, H., W. P. Arnott, C. F. Rogers, J. C. Chow, L. E. Sherman, and D. L. Dietrich, 1998: Photoacoustic and filter measurements related to aerosol light absorption during the Northern Front Range Air Quality Study. *J. Geophys. Res.,* **103,** 28 149–28 157.

Öström, E., and K. J. Noone, 2000: Vertical profiles of aerosol scattering and absorption measured in situ during the North Atlantic Aerosol Characterization Experiment ACE-2. *Tellus,* **52B,** 526–545.

Pilewskie, P., M. Rabbette, R. Bergstrom, J. Marquez, B. Schmid, and P. B. Russell, 2000: The discrepancy between measured and modeled downwelling solar irradiance at the ground: Dependence on water vapor. *Geophys. Res. Lett.,* **27,** 137–140.

Podgorny, I. A., W. Conant, V. Ramanathan, and S. K. Satheesh, 2000: Aerosol modulation of atmospheric and surface solar heating over the tropical Indian Ocean. *Tellus,* **52B,** 947–958.

Quinn, P., and Coauthors, 2000: A comparison of aerosol chemical and optical properties from the 1st and 2nd Aerosol Characterization Experiments. *Tellus,* **52B,** 239–257.

Raes, F., T. Bates, F. McGovern, M. van Liedekerke, 2000: The 2nd Aerosol Characterization Experiment (ACE-2): General overview and main results. *Tellus,* **52B,** 111–125.

Redemann, J., and Coauthors, 2000a: Retrieving the vertical structure of the effective aerosol complex index of refraction from a combination of aerosol in situ and remote sensing measurements during TARFOX. *J. Geophys. Res.,* **105,** 9949–9970.

——, R. P. Turco, K. N. Liou, P. V. Hobbs, R. W. Bergstrom, E. V. Browell, and P. B. Russell, 2000b: Case studies of the vertical structure of the shortwave direct aerosol radiative forcing during TARFOX. *J. Geophys. Res.,* **105,** 9971–9979.

——, P. B. Russell, and P. Hamill, 2001: Dependence of aerosol light absorption and single scattering albedo on ambient relative humidity for sulfate aerosols with black carbon cores. *J. Geophys. Res.,* **106,** 27 485–27 495.

Remer, L. A., and Y. Kaufman, 1998: Dynamic aerosol model: Urban/industrial aerosol. *J. Geophys. Res.,* **103,** 13 859–13 871.

——, ——, and B. N. Holben, 1999: Interannual variation of ambient aerosol characteristics on the east coast of the United States. *J. Geophys. Res.,* **104,** 2223–2231.

Russell, P. B., and J. Heintzenberg, 2000: An overview of the ACE-2 Clear Sky Column Closure Experiment (CLEARCOLUMN). *Tellus,* **52B,** 463–483.

——, S. Kinne, and R. Bergstrom, 1997: Aerosol climate effects: Local radiative forcing and column closure experiments. *J. Geophys. Res.,* **102,** 9397–9407.

——, P. V. Hobbs, and L. L. Stowe, 1999a: Aerosol properties and radiative effects in the United States east coast haze plume: An overview of the Tropospheric Aerosol Radiative Forcing Observational Experiment (TARFOX). *J. Geophys. Res.,* **104,** 2213–2222.

——, and Coauthors, 1999b: Aerosol-induced radiative flux changes off the United States mid-Atlantic coast: Comparison of values calculated from sun photometer and in situ data with those measured by airborne pyranometer. *J. Geophys. Res.,* **104,** 2289–2307.

Sokolik, I., and O. B. Toon, 1997: Direct radiative forcing by anthropogenic airborne mineral aerosols. *Nature,* **381,** 681–685.

Stowe, L. I., A. M. Ignatov, and R. R. Singh, 1997: Development, validation, and potential enhancements to the second-generation operational aerosol product at the National Environmental Satellite, Data, and Information Service of the National Oceanic and Atmospheric Administration. *J. Geophys. Res.,* **102,** 16 923–16 934.

Swietlicki, E., andand Coauthors, 2000: Hygroscopic properties of aerosol particles in the north-eastern Atlantic during ACE-2. *Tellus,* **52B,** 201–227 .